

# X-ray Clusters of Galaxies as Tracers of Structure in the Universe

Stefano Borgani<sup>1</sup> & Luigi Guzzo<sup>2</sup>

<sup>1</sup> INFN, Sezione di Trieste  
c/o Dipartimento di Astronomia dell'Università,  
Via Tiepolo 11, I-34131, Trieste, Italy\*  
borgani@ts.astro.it

<sup>2</sup> Osservatorio Astronomico di Brera  
Via Bianchi 46, I-23807, Merate, Italy  
guzzo@merate.mi.astro.it

*To appear as a review in Nature  
4 January 2001 issue*

Clusters of galaxies outline the network of the distribution of visible matter in the Universe, marking the highest-mass knots where filamentary structures join together. If we observe the sky in  $X$  rays, clusters of galaxies stand out as cosmic lighthouses by virtue of a thin gas trapped and heated within their gravitational potential wells. This powerful emission is directly linked to the total gravitating mass they contain, such that they can be efficiently used as tracers of the cosmic mass distribution within a sizeable fraction of the observable Universe. Recent observational

---

\*also, INFN, Sezione di Perugia, Perugia, Italy

campaigns have for the first time used  $X$ -ray clusters to map cosmic structures on scales approaching 3 billion light years. The emerging picture is remarkably consistent with the expectation of a low-density Universe dominated by cold dark matter.

The present-day appearance of the galaxy distribution is the result of the gravitational growth of the initial fluctuations laid down during the very early stages of cosmic history, coupled to dissipative processes which lit up matter and made it visible to our telescopes. Cosmological models directly predict the distribution and gravitational growth of the mass, not of the light we actually observe from galaxies. Thus, the grand challenge of unveiling the nature of cosmic initial conditions from the observed structure of the Universe is a process which is ideally characterised by two steps. The first involves constructing maps of the distribution of luminous objects on sufficiently large scales, so as to encompass a representative portion of the whole Universe. The second requires relating such “light maps” to the underlying mass through a physically motivated and robust recipe, the two distributions being in principle not related by a one-to-one correspondence. Although nowadays galaxy surveys are able to probe the distribution of luminous structures over scales larger than 100 Megaparsecs (Mpc, 1 pc=3.26 light years), their relation to the actual mass distribution depends on the still poorly understood physics of galaxy formation and evolution.

Clusters of galaxies, the most evident concentrations in galaxy maps, can themselves be used as tracers of the large-scale structure of the Universe. While missing the fine details, they can be efficiently used to study extremely large volumes at a reduced cost in terms of telescope time with respect to fully-sampled galaxy surveys. Already the earliest statistical samples of clusters from visually-compiled catalogues [1, 2, 3] reached typical depths of few hundreds Mpc, and the Abell catalogue in particular [1] represents still today one of the main resources for cosmological studies (e.g. [6, 7]). It is within the “gravitational sinks” of galaxy clusters that evidence for the elusive dark matter was first found in the thirties [4, 5], as a necessary ingredient to explain the fast motions observed for

cluster galaxies.

The loose definition of a cluster as a collection of galaxies is however intrinsically uncertain, definitely not optimal for estimating its mass, as required for linking observations and theoretical predictions. Fortunately, about 20–30% of the optically invisible mass of a cluster is in the form of a diffuse hot gas [8], trapped and heated to a temperature of the order of  $10^8$  K by its gravitational potential. At such high temperatures, this gas is a fully ionised plasma, producing a powerful  $X$ -ray emission by free–free electron–ion interactions, the so-called *bremsstrahlung* radiation. With total luminosities of  $\sim 10^{43} - 10^{45}$  erg s $^{-1}$ , and large physical dimensions ( $\sim 1$  Mpc), galaxy clusters can be recognised over the rather sparse  $X$ -ray sky [9] as extended sources, out to very large distances. The  $X$ -ray luminosity is shown to correlate well with the cluster mass and indeed provides a fairly direct way to make a robust comparison of the observed clustering with the predictions of cosmological models. The most recent projects finalised to study large-scale structure benefiting of these advantages [10, 11, 12, 13, 14], are based on the all-sky survey by the ROSAT satellite and have so far accumulated distances for  $\sim 1000$  clusters within a volume with size of the order of 1000 Mpc. The degree of clumpiness observed in these samples on scales of several hundreds Mpc is remarkable, and larger than previously indicated by galaxy surveys. Very interestingly, the amplitude and shape of the corresponding distribution of mass inhomogeneities, which for  $X$ -ray clusters can be precisely computed, point toward the picture of a Universe dominated by non-baryonic cold dark matter, whose density is about one third of that necessary for it to recollapse under its own self-gravity. Coupled to the recent strong evidence for a nearly flat spatial geometry from the anisotropy of the Cosmic Microwave Background [15, 16], this reinforces the apparent need for an extra cosmic energy, what is commonly associated with the cosmological constant.

## Large-scale view of the Universe

Modern cosmology uses the distribution of galaxies and clusters to map the structure of the Universe on scales which have presently reached a few  $100 h^{-1}\text{Mpc}$  (here  $h$  is the Hubble constant,  $H_0$ , in units of  $100 \text{ km s}^{-1} \text{ Mpc}^{-1}$ ; see Box 1). First systematic *redshift surveys* of galaxies started around the half of the seventies [18] and became an industry during the last two decades (see ref. [17] and references therein; also, see Box 1 for the definition of redshift). The main features of the large-scale distribution of galaxies emerging from these cosmic maps include long, thin superclusters, with stronger concentrations – rich clusters – located at their intersections, surrounding large regions essentially devoid of galaxies. This is explicitly illustrated by the top panel of Fig. 1, where we have plotted the distribution of about 26,000 galaxies composing the Las Campanas Redshift Survey (LCRS, blue points) [19]. The evident inhomogeneity in the distribution of galaxies can be statistically quantified at the simplest level in terms of their *two-point correlation function*  $\xi(r)$ , which measures the excess probability with respect to a random distribution, to observe a pair of galaxies separated by a distance  $r$  [20] (see Box 1). The squares in Fig. 2 shows the correlation function measured from the LCRS galaxy survey [21]. Consistently with other samples of normal galaxies,  $\xi(r)$  is well described by a power-law  $(r/r_o)^{-\gamma}$ , with  $r_o \simeq 5 h^{-1}\text{Mpc}$  and  $\gamma \simeq 1.8$  for separations  $r$  between about 0.1 and  $10 h^{-1}\text{Mpc}$ . This roughly tells us that galaxies are strongly clustered within these two decades of scales, while tending to a more homogeneous distribution at larger separations [22, 23, 24].

This variety of observed cosmic structures is interpreted as arising from the gravitational growth of initially tiny fluctuations, generated in the early stages of the life of the Universe [25, 26]. Cosmological models yield predictions for the character of such initial fluctuations in terms of their *power spectrum*  $P(k)$ , i.e. the Fourier transform of  $\xi(r)$  (see Fig. 3 and Box 1). However, their connection to the observations is not trivial. While direct and reliable predictions can be

made about the distribution of matter concentrations of a given mass [28], it is far less straightforward to describe the clustering properties of the galaxies which have then formed within these potential wells. A suitable recipe to relate their observable characteristics (as luminosity, colour and morphology) to their actual total mass, would in fact require a complete understanding of all physical processes regulating the formation and evolution of stars within galaxies. Although intensive work is currently dedicated to a better comprehension of such mechanisms (e.g., [29, 30] and references therein), this is far from being satisfactory.

## Clusters as tracers of the cosmic web

Once we accept the idea of luminous objects as tracers of the underlying mass structure of the Universe, we might think to alternatives to using single galaxies for this scope. The bottom panel in Fig. 1 plots the distribution of a large sample of clusters of galaxies[13, 31] detected by the X-ray satellite ROSAT, one typical example of which is shown in the combined optical–X–ray picture of Fig. 4. Comparison of the two panels of Fig. 1 gives an idea of how massive clusters provide a coarser mapping of large–scale structure, but are very efficient to sample extremely large ( $r > 100 h^{-1}\text{Mpc}$ ) volumes, which translates into a more modest investment of telescope time to reconstruct their 3D distribution. In general, rich clusters as that of Fig. 4 contain several hundreds of galaxies within a typical size of  $\sim 1 h^{-1} \text{ Mpc}$ , and represent the largest gravitationally bound structures in the Universe. Galaxies in clusters are observed to move along their orbits with a typical line–of–sight velocity dispersion  $\sigma_v \sim 1000 \text{ km s}^{-1}$ , so that the time required to a galaxy to cross the cluster is approximately  $t_{cr} = r/\sigma_v \sim 10^9 \text{ yr}$ . This means that, given the typical age of the Universe,  $t_U \simeq H_0^{-1} \simeq 10^{10} h^{-1} \text{ yrs}$ , rich clusters had enough time to evolve into dynamically relaxed systems. While a continuous infall of galaxies moving along radial orbits takes place in the cluster outskirts, the central regions have therefore reached virial equilibrium,

in which the total mass is related to the galaxy velocity dispersion as  $M_{vir} \simeq 3\sigma_v^2 r/G \sim 10^{15} h^{-1} M_\odot$ . Already first pioneering attempts [4, 5] showed that cluster masses measured in this way are about ten-times larger than expected from the sum of the masses of the individual member galaxies. This observation represented the earliest evidence for a “hidden” form of matter permeating the Universe.

In Figs. 2 and 3 we have also plotted the correlation function and power spectrum measured for clusters selected through their  $X$ -ray emission [32, 33]. Both figures show how clusters display a clustering amplitude significantly larger than galaxies, while maintaining a similar shape: the correlation length of  $X$ -ray luminous clusters is roughly 4 times larger,  $r_o \simeq 20 h^{-1} \text{Mpc}$ . This gives us an explicit demonstration of how changing the kind of tracer we are using, we measure different clustering properties. When first observed in optically-selected samples [34, 35, 36] this motivated the concept of *bias* in the distribution of cosmic structures [37]: the strong clumpiness of the cluster distribution is just the natural consequence of clusters tracing only the high-density peaks of the underlying mass density field. More in general, in the cosmologists’ jargon, the word “bias” is meant to indicate the relation between the distribution of a given class of observable objects, like galaxies and clusters, and the underlying distribution of matter: *what regulates the amount of clustering of a class of objects is just the characteristic mass of the objects themselves*. In the case of clusters, their correlation function and power spectrum are predicted to be amplified with respect to those of the matter distribution, by a constant *biasing* factor, whose value is uniquely known once the cluster mass and the cosmological model are specified [28]. This has the important consequence that, given a sample of clusters selected according to their mass, the observed clustering is a truly direct test of the cosmological model. Surprising as it might seem to the reader, despite clusters are evidently more “biased” tracers of the mass distribution with respect to galaxies, they are more effective because their biasing factor can be more easily computed.

Such a theoretical simplicity has however to face the somewhat loose visual definition of a cluster as an agglomerate of galaxies. The traditional way of selecting clusters is in fact based on the “eyeball” detection of overdensities in the projected galaxy distribution on the sky [1]. In the attempt to provide a simple estimator of the cluster mass, a *richness* is measured by counting, within a fiducial aperture radius, the number of galaxies which belong to the cluster. However, partly for the difficulty of properly correcting for the contamination by background and foreground galaxy counts [38, 39], the richness itself is intrinsically a poor mass indicator when compared to  $X$ –ray luminosity (see Fig. 5). This highlights the difficulty of using the distribution of clusters selected by optical richness to quantitatively constrain theoretical scenarios for the formation of cosmic structures.

## Clusters in $X$ –rays

The first  $X$ –ray observations of nearby galaxy clusters [41, 42, 44] showed that they are in general associated with extended  $X$ –ray sources [43], with luminosities  $L_X$  in the range  $\sim 10^{43}$ – $10^{45}$  erg s $^{-1}$ , whose emission originates in a diffuse hot intergalactic medium permeating the cluster potential well (see [45], for a historical review). Since at equilibrium gas and galaxies in the cluster have to share the same dynamics, one expects to measure a gas temperature  $k_B T \simeq \mu m_p \sigma_v^2$ , where  $m_p$  is the proton mass and  $\mu \simeq 0.6$  is the gas mean molecular weight. Given the typical cluster velocity dispersions, this corresponds to a temperature of a few keV, which is what is indeed measured by  $X$ –ray observations. At such energies the intra–cluster medium (ICM), which is composed mainly by hydrogen, behaves like a fully ionised plasma with an atomic density of  $\sim 10^{-3}$  particles per cm $^3$ . The scattering between free electrons and ions in such conditions produces a *thermal bremsstrahlung* radiation, which peaks in the  $X$ –ray region of the electromagnetic spectrum. For this mechanism, the emissivity (i.e., the energy released per unit time, frequency and volume) at frequency  $\nu$  and temperature

$T$  scales as  $\epsilon_\nu \propto n_e n_i T^{-1/2} \exp(-h_P \nu / k_B T)$ , where  $n_e$  and  $n_i$  are the number densities of electrons and ions, respectively, and  $h_P$  is the Planck constant. This expression shows why the identification of clusters in the  $X$ -ray band is less affected by projection effects with respect to the optical selection based on galaxy overdensities: while the optical emission depends linearly on the number of galaxies, the  $X$ -ray emission depends on the square of the local gas density, making clusters stand out more sharply in the  $X$ -ray than in the optical light. The contours in Fig. 4 explicitly show how in the  $X$ -ray band the cluster emerges as a single, practically isolated, extended source.

The  $X$ -ray luminosity of galaxy clusters is a direct function of the total cluster mass, at least in a phenomenological way [46], as demonstrated by the plot in the bottom panel of Fig. 5. This is further supported by the observation of a well-defined relation between the  $X$ -ray luminosity and the temperature of the ICM, the latter being a reliable indicator of the depth of the cluster gravitational potential [56, 57]. Such a relationship has been observationally calibrated at low redshift with a fairly large number of clusters, showing that  $L_X \propto T^\alpha$  with  $\alpha \simeq 3$ , a small scatter,  $\lesssim 30\%$ , around this relation [58, 59]. and no evidence for evolution out to  $z \simeq 1.3$  [60, 61, 62, 63]. These observations have profound implications for the physics of the ICM, as the steep slope of the luminosity-temperature relation and the lack of evolution can not be accounted for by the action of gravity only. Additional physical mechanisms, like radiative cooling in the central cluster regions and heating from supernovae explosions and active galactic nuclei, seem to play a key role in the thermodynamics of the intra-cluster gas (e.g., [64, 65], and references therein). It is worth emphasizing that, whichever mechanism determines the ICM thermodynamics, the very fact that gas temperature and luminosity are observed to be closely correlated demonstrates that  $L_X$  is indeed a reliable diagnostic of the cluster mass.

Besides  $X$ -ray imaging, radio observations of the Sunyaev-Zel'dovich (SZ) effect are becoming an important alternative method to detect distant clusters with a well-defined mass selection (see [66] and [67] for recent reviews). The



SZ effect is observed as a surface brightness variation in the Cosmic Microwave Background (CMB) in the direction of a galaxy cluster and is produced by the scattering of CMB photons on the energetic electrons of the ICM (what is known as *inverse Compton*). Owing to its nature, the SZ signal depends only on the total thermal energy of the ICM, and is less sensitive than the  $X$ -ray emission to its detailed structure and complexity. Although the SZ signal has been now detected for several known clusters, no systematic blind search based on this effect has been realized to date. The extensive use of this technique for large-scale structure studies will become feasible only with the next generation of high-resolution micro-wave surveyors, as the Planck satellite.

## Clustering of $X$ -ray clusters and implications for cosmology

A quantitative measure of the clustering of  $X$ -ray clusters has been possible only in recent years, and on rather pioneeristic samples [47]. A major leap forward has been provided by the ROSAT All-Sky Survey (RASS, [48]), which for the first time provided a  $X$ -ray imaging survey of the whole sky, in which thousands of clusters as faint as  $f_X = 10^{-12} \text{erg s}^{-1} \text{cm}^{-2}$  can be detected<sup>1</sup>. Early studies of  $X$ -ray clusters identified within sub-regions of the RASS produced first estimates of the clustering of these objects [49, 50, 51, 52]. The quality of such  $X$ -ray cluster catalogues has substantially improved through the recent completion of the optical identification and redshift measurement for a statistically complete sample of nearly 500 RASS clusters over half of the sky [13, 31] (see also Fig. 1). Benefitting of the precision intrinsic to the  $X$ -ray selection, these data are now providing an unprecedented large-scale description of the structure of the Universe and a powerful testbed for cosmological scenarios. Figs. 2 and 3 highlight the accuracy with which the clustering of clusters is now

---

<sup>1</sup>Depending on the technology of their mirrors and detectors, different  $X$ -ray satellites cover different energy ranges, which need to be specified when quoting fluxes and luminosities. The ROSAT band used here covers the energy range 0.1–2.4 keV.

measured on intermediate scales ( $\sim 10\text{--}100 h^{-1}\text{Mpc}$ ) by the correlation function [32] and on the largest scales achievable to date ( $\sim 500 h^{-1}\text{Mpc}$ ) with the power spectrum [33]. Extension of this work to the whole sky [14] and to fainter fluxes will eventually result in a complete sample of about 1500 clusters at a median redshift  $z \simeq 0.1$ .

Given the well-defined  $X$ -ray selection function for these samples, the interpretation of the observed clustering in terms of cosmological models is now relatively straightforward. Once the gravitational growth of cluster-sized mass clumps within a given model is predicted, either analytically [28, 55] or numerically [53, 54], then the corresponding  $X$ -ray emission from the ICM can be computed using the mass-temperature-luminosity relation discussed in the previous section. Fig. 6 is an illustrative example of the development of cosmic structures as generated by a modern numerical  $N$ -body experiment, simulating the gravitational growth of clustering from given initial conditions and capable to precisely resolve individual cluster-sized clumps while at the same time following their distribution on scales of several hundreds Megaparsecs. The mass-luminosity connection makes it possible to compute the correlation function and power spectrum that clusters with a given  $X$ -ray luminosity are predicted to have in each model [51, 52, 33, 32]. Remarkably, the amplitude of the correlation function and the scales over which clusters are observed to be still inhomogeneously distributed, consistently require a low-density Universe dominated by cold dark matter (CDM), with density parameter  $\Omega_m \sim 0.3$ . This is illustrated by the two curves in Figs. 2 and 3, chosen to be both consistent with CMB anisotropies on small [15, 16] and large [68] angular scales, but with different  $\Omega_m$ . Even a small increase of the density parameter from 0.3 to 0.5 produces a clear lack of coherence on scales above  $100 h^{-1}\text{Mpc}$ . This gives an idea not only of the quality reached by current data, but also of the role future surveys of  $X$ -ray clusters could play in the framework of next decade high-precision cosmology, when observations at different wavelengths will combine to pin down the values of cosmological parameters with high accuracy (e.g. [69]).

## Clusters and the evolution of the Universe

We have marked in Fig. 6 the positions of clusters with a mass corresponding to a temperature larger than 3 keV, which translates into a luminosity of about  $10^{44} \text{ erg s}^{-1}$ . The two  $z > 0$  snapshots correspond to look-back times of 5.7 and 9.0 billion years for the L03 cosmology and to 6.6 and 9.5 billion years for the EdS cosmology. Despite the similar pattern produced at the present time ( $z = 0$ ), the past histories of the two models are very different. The most striking feature is probably the fast decay in the abundance of hot, massive clusters as a function of redshift in the  $\Omega_m = 1$  model, in contrast to the mild changes visible in the low-density model. This remarkable evolutionary difference represents one of the major motivations for the recent deep  $X$ -ray searches of clusters down to fluxes about 1/100 that of the RASS (see refs. [70, 71] and references therein). Clusters at  $z \simeq 0.5$  are nowadays not considered as exceptions and even few examples of  $z \gtrsim 1$   $X$ -ray bright clusters are now known [72]. The major result reached by these surveys is the evidence for a weak evolution of the bulk of the cluster population out to  $z \simeq 1$ , again consistent with the picture of a low- $\Omega_m$  Universe.

Besides the cluster number density – which basically measures the degree of initial inhomogeneity on scales  $\lesssim 10 h^{-1} \text{ Mpc}$  – the large-scale pattern also evolves in a markedly different way between the two models of Fig. 6, this difference being mainly driven by the value of the density parameter [73, 74] (see Box 1). Could we follow this evolution back in redshift using available  $X$ -ray selected clusters? Unfortunately, this is not yet possible: even the largest deep surveys contain only  $\sim 100$  clusters within relatively small patches spread over the whole sky, which gives no chance to map their distribution within a sufficiently large contiguous volume at redshift  $z > 0.3$ . For this to be possible, a large-area  $X$ -ray survey would be needed, reaching a flux limit significantly fainter than the ROSAT All Sky Survey<sup>2</sup>.

---

<sup>2</sup> For example, detecting a typical cluster with  $X$ -ray luminosity  $L_X \sim 10^{44} h^{-2} \text{ erg}$

A strong progress in  $X$ -ray astronomy is foreseen for the next few years, in relation to the newly-launched AXAF-Chandra and XMM-Newton  $X$ -ray satellites. Also, new improved  $X$ -ray observatories are currently under study [75]. Still, none of these missions will be ideal for extended studies of large-scale structure, as they are not designed to perform an all-sky survey, or at least to cover a large enough ( $\sim 1000$  sq. deg.) contiguous area. Covering the whole sky in a reasonable time and with about 100 times higher sensitivity than the ROSAT All-Sky Survey would be feasible even now, given current advances in the technology of  $X$ -ray optics [76]. An all-sky survey to this depth would contain more than 100,000 clusters out to  $z \sim 1$ , with about 15,000 of these laying above  $z \gtrsim 0.5$ . Although no such experiment is currently funded, several ideas and proposals are circulating in the scientific community. We can hope that the enormous potential of  $X$ -ray clusters to follow the shaping process of the Universe will soon make these projects become reality.

## References

- [1] Abell, G.O. The Distribution of Rich Clusters of Galaxies. *Astrophys. J. Suppl.* **3**, 211–278 (1958).
- [2] Abell, G.O., Corwin, H.G.Jr. & Olowin, R.P. A catalog of rich clusters of galaxies. *Astrophys. J. Suppl.* **70**, 1–138 (1989).
- [3] Zwicky, F., Herzog, E., Wild, P., Karpowicz, M., & Kowal, C. *Catalogue of Galaxies and of Clusters of Galaxies* (Pasadena: California Institute of Technology) (1961-68)
- [4] Zwicky, F. *Helvetica Physica Acta*, **6**, 110 (1933).
- [5] Smith, S. The mass of the virgo cluster. *Astrophys. J.* **83**, 23–30 (1936).

---

$s^{-1}$  at redshift  $z \simeq 1$ , requires a survey limiting flux about 1/100 of that of the RASS.

- [6] Retzlaff, J., Borgani, S., Gottlöber, S., Klypin A. & Müller, V. Constraining cosmological models with cluster power spectra. *New Astron.* **3**, 631–646 (1998).
- [7] Miller, C.J., & Batuski, D.J. The Power Spectrum of rich clusters to scales approaching 1000 Mpc. *Astrophys. J.* (submitted, preprint astro-ph/0002295)
- [8] Evrard, A.E. The intracluster gas fraction in X-ray clusters - Constraints on the clustered mass density. *Mon. Not. R. Astron. Soc.* **292**, 289–297 (1997).
- [9] Hasinger, G., Burg, R., Giacconi, R., Schmidt, M., Trumper, J. & Zamorani, G. The ROSAT Deep Survey. I. X-ray sources in the Lockman Field. *Astron. Astrophys.* **329**, 482–494 (1998).
- [10] Ebeling, H., Edge, A.C., Allen, S.W., Crawford, C.S., Fabian, A.C. & Huchra, J.P. Properties of the X-ray-brightest Abell-type clusters of galaxies (XBACs) from ROSAT All-Sky Survey data - I. The sample. *Mon. Not. R. Astron. Soc.* **281**, 799–829 (1996).
- [11] Ebeling, H., Edge, A.C., Böhringer, H., Allen, S.W., Crawford, C.S., Fabian, A.C., Voges, W., & Huchra, J.P. The ROSAT Brightest Cluster Sample - I. The compilation of the sample and the cluster log N-log S distribution. *Mon. Not. R. Astron. Soc.* **301**, 881–914 (1998).
- [12] De Grandi, S., Böhringer, H., Guzzo, L., Molendi, S., Chincarini, G., Collins, C.A., Cruddace, R., Neumann, D., Schindler, S., Schuecker, P., & Voges, W. A Flux-limited Sample of Bright Clusters of Galaxies from the Southern Part of the ROSAT All-Sky Survey: The Catalog and LOG N-LOG S. *Astrophys. J.* **514**, 148–163 (1999).

- [13] Böhringer, H., et al. (the REFLEX Team) The ROSAT ESO Flux-Limited X-ray (REFLEX) galaxy cluster survey I: The construction of the cluster sample *Astron. Astrophys.* (submitted, preprint astro-ph/0012266).
- [14] Böhringer, H., Voges, W., Huchra, J.P., et al. The Northern ROSAT All-Sky (NORAS) Galaxy Cluster Survey I: X-ray Properties of Clusters Detected as Extended X-ray Sources. *Astrophys. J. Suppl.* **129**, 435–474 (2000).
- [15] de Bernardis, P., et al. (BOOMERANG Collaboration) A flat Universe from high-resolution maps of the cosmic microwave background radiation. *Nature* **404**, 955–959 (2000).
- [16] Balbi, A., et al. (MAXIMA Collaboration) Constraints on Cosmological Parameters from MAXIMA-1. *Astrophys. J. Lett.* **545** 1–4 (2000).
- [17] Guzzo, L. Large-scale structure at the turn of the Millennium. *Proceedings of the XIX Texas Symposium on Relativistic Astrophysics & Cosmology*, Nucl. Phys. B (Proc. Suppl.) 80, E. Aubourg et al. eds., (2000), p.233-09/06 (preprint astro-ph/9911115).
- [18] Rood, H.J. Voids. *Ann. Rev. Astron. Astrophys.* **26**, 245–294 (1988).
- [19] Shectman, S.A., Landy, S.D., Oemler, A., Tucker, D.L., Lin, H., Kirshner, R.P. & Schechter, P.L. The Las Campanas Redshift Survey. *Astrophys. J.* **470**, 172–188 (1996).
- [20] Peebles, P.J.E. *Principles of Physical Cosmology* (Princeton: Princeton University Press) (1993).
- [21] Tucker, D.L., Oemler, A., Kirshner, R.P., Lin, H., Shectman, S.A., et al. The Las Campanas Redshift Survey galaxy-galaxy autocorrelation function. *Mon. Not. R. Astr. Soc.* **285**, L5–L9 (1997).

- [22] Borgani, S. Scaling in the Universe. *Phys. Rep.* **251**, 1–152 (1995).
- [23] Guzzo, L. Is the Universe homogeneous? (on large scales). *New Astron.* **2**, 517–532 (1997).
- [24] Wu, K., Lahav, O. & Rees, M.J. The large-scale smoothness of the Universe. *Nature* **397**, 225–230 (1999).
- [25] Peacock, J.A., *Cosmological Physics* (Cambridge University Press, Cambridge) (1999).
- [26] Coles, P. & Lucchin, F. *Cosmology. The origin and evolution of cosmic structure.* (Chichester: Wiley) (1995).
- [27] Lin, H., Kirshner, R.P., Sheckman, S.A., Landy, S.D., Oemler, A., Tucker, D.L. & Schechter, P.L. The Power Spectrum of Galaxy Clustering in the Las Campanas Redshift Survey. *Astrophys. J.* **471**, 617–635 (1996).
- [28] Mo, H.J. & White S.D.M. An analytic model for the spatial clustering of dark matter haloes. *Mon. Not. R. Astron. Soc.* **282**, 347–361 (1996).
- [29] Somerville, R.S. & Primack, J.R. Semi-analytic modelling of galaxy formation: the local Universe. *Mon. Not. R. Astron. Soc.* **310**, 1087–1110 (1999).
- [30] Benson, A.J., Cole, S., Frenk, C.S., Bough, C.M. & Lacey, C.G. The nature of galaxy bias and clustering. *Mon. Not. R. Astr. Soc.* **311**, 793–808 (2000).
- [31] Guzzo, L., Böhringer, H., Schuecker, P., Collins, C.A., Schindler, S., et al (the REFLEX Team) The REFLEX Cluster Survey: observing strategy and first results on large-scale structure. *The Messenger* **95**, 27–32 (1999).

- [32] Collins, C.A., Guzzo, L., Böhringer, H. Schuecker, P., Chincarini, G., et al. (the REFLEX Team), The REFLEX Galaxy Cluster Survey II. The spatial correlation function. *Mon. Not. R. Astron. Soc.* **319**, 939–948 (2000).
- [33] Schuecker, P., Böhringer, H., Guzzo, L., Collins, C.A., et al. (the REFLEX Team) The REFLEX Galaxy Cluster Survey III. The Power Spectrum. *Astron. Astrophys.* (submitted, preprint astro-ph/0012105).
- [34] Bahcall, N.A. & Soneira, R.M. The spatial correlation function of rich clusters of galaxies. *Astrophys. J.* **270**, 20–38 (1983).
- [35] Klypin, A.A. & Kopylov, A.I. The Spatial Covariance Function for Rich Clusters of Galaxies. *Sov. Astron. Lett.* **9**, 41–44 (1983).
- [36] Postman, M. Clusters as Tracers of Large Scale Structure. *Evolution of Large-Scale Structure: from Recombination to Garching* (T. Banday & R. Sheth eds.) p.23 (1988).
- [37] Kaiser, N. On the spatial correlations of Abell clusters. *Astrophys. J.* **284**, L9–L12 (1984).
- [38] Lumsden, S.L., Nichol, R.C., Collins, C.A. & Guzzo L. The Edinburgh-Durham Southern Galaxy Catalogue. IV - The Cluster Catalogue. *Mon. Not. R. Astron. Soc.* **258**, 1–22 (1992).
- [39] Eke, V.R., Cole, S., Frenk, C.S. & Navarro, J.F. Cluster correlation functions in N-body simulations. *Mon. Not R. Astron. Soc.* **281**, 703–715 (1996).
- [40] Girardi, M., Giuricin, G., Mardirossian, F., Mezzetti, M. & Boschin, W. Optical Mass Estimates of Galaxy Clusters. *Astrophys. J.* **505**, 74–95 (1998).



- [41] Kellogg, E., Gursky, H., Leong, C., Schreier, E., Tananbaum, H. & Giacconi, R. *X*-ray observations of the Virgo cluster, NGC 5128, and 3C 273 from the UHURU satellite. *Astrophys. J. Lett.* **165**, L49–L52 (1971).
- [42] Gursky, H., Kellogg, E.M., Murray, S., Leong, C., Tananbaum, H. & Giacconi, R. A Strong X-Ray Source in the Coma Cluster Observed by UHURU. *Astrophys. J. Lett.* **167**, L81–L84 (1971).
- [43] Cavaliere, A., Gursky, H. & Tucker, W.H. Extragalactic *X*-Ray Sources and Associations of Galaxies. *Nature* **231**, 437–438 (1971).
- [44] Giacconi, R., Murray, S., Gursky, H., Kellogg, E., Schreier, T., Matilsky, T., Koch, D. & Tananbaum, H. The Third UHURU Catalog of *X*-Ray Sources. *Astrophys. J. Suppl.* **27**, 37–64 (1974).
- [45] Sarazin, C. *X-Ray Emission from Clusters of Galaxies* (Cambridge: Cambridge University Press) (1988).
- [46] Reiprich, T.H. & Böhringer, H. The empirical X-ray luminosity-gravitational mass relation for clusters of galaxies. *Astr. Nachr.* **320**, 296–299 (1999).
- [47] Lahav, O., Edge, A.C., Fabian, A.C. & Putney, A. The spatial distribution of X-ray clusters of galaxies. *Mon. Not. R. Astr. Soc.* **238**, 881–895 (1989).
- [48] Voges, W., Boller, T., Dennerl, K., et al. Identification of the ROSAT All-Sky Survey Sources. *Röntgenstrahlung from the Universe*, (H.U. Zimmermann, J.E. Trümper, H. Yorke eds.), MPE Report No. 263, p. 637 (1996).
- [49] Romer, A.K., Collins, C.S., Böhringer, H., Cruddace, R.G., Ebeling, H., MacGillivray, H.T. & Voges, W. The Large-Scale Distribution of *X*-Ray Clusters of Galaxies. *Nature* **372**, 75–77 (1994).

- [50] Nichol, R.C., Briel, O.G., & Henry, J.P. The spatial correlation function from an *X*-ray selected sample of Abell clusters. *Mon. Not. R. Astron. Soc.* **267**, 771–778 (1994)
- [51] Borgani, S., Plionis, M., & Kolokotronis, V. Cosmological constraints from the clustering properties of the *X*-ray Brightest Abell-type Cluster sample. *Mon. Not. R. Astron. Soc.* **305**, 866–874 (1999).
- [52] Moscardini, L., Matarrese, S., De Grandi, S. & Lucchin, F. The correlation function of *X*-ray galaxy clusters in the ROSAT All-Sky Survey 1 Bright Sample. *Mon. Not. R. Astron. Soc.* **314**, 647–656 (2000).
- [53] Governato, F., Babul, A., Quinn, T., Tozzi, P., Baugh, C.M., Katz, N. & Lake, G. Properties of galaxy clusters: mass and correlation functions. *Mon. Not. R. Astr. Soc.* **307**, 949–966 (1999).
- [54] Colberg, J.M., et al. Clustering of Galaxy Clusters in CDM Universes. *Mon. Not. R. Astr. Soc.*, **316**, 283–298 (2000).
- [55] Sheth, R.K., Mo, H.J. & Tormen, G. Ellipsoidal collapse and an improved model for the number and spatial distribution of dark matter haloes. *Mon. Not. R. Astron. Soc.* (submitted, preprint astro-ph/9907024).
- [56] Evrard, A.E., Metzler, C.A. & Navarro, J.F. Mass Estimates of *X*-Ray Clusters. *Astrophys. J.* **469**, 494–507 (1996).
- [57] Bryan, G.L. & Norman M.L. Statistical Properties of *X*-Ray Clusters: Analytic and Numerical Comparisons. *Astrophys. J.* **495**, 80–99 (1998).
- [58] White, D.A., Jones, C. & Forman, W. An investigation of cooling flows and general cluster properties from an *X*-ray image deprojection analysis of 207 clusters of galaxies. *Mon. Not. R. Astr. Soc.* **292**, 419–467 (1997).

- [59] Arnaud, M. & Evrard, A.E. The  $L_X$ - $T$  relation and intracluster gas fractions of X-ray clusters. *Mon. Not. R. Astr. Soc.* **305**, 631–640 (1999).
- [60] Mushotzky, R.F. & Scharf, C.A. The Luminosity-Temperature Relation at  $z = 0.4$  for Clusters of Galaxies. *Astrophys. J. Lett.* **482**, L13–L16 (1997).
- [61] Della Ceca, R., Scaramella, R., Gioia, I.M., Rosati, P., Fiore, F. & Squires, G. BeppoSAX observations of two high redshift clusters of galaxies: RXJ 0152.7-1357 and MS 2053.7-0449. *Astron. Astrophys.* **353**, 498–506 (2000).
- [62] Henry, P. Measuring Cosmological Parameters from the Evolution of Cluster  $X$ -Ray Temperatures. *Astrophys. J.* **534**, 565–580 (2000).
- [63] Borgani, S. *et al.* Measuring  $\Omega_m$  with the ROSAT Deep Cluster Survey *Astrophys. J.* (submitted) (2001).
- [64] Tozzi, P. & Norman, C. The Evolution of  $X$ -Ray Clusters and the Entropy of the Intra Cluster Medium. *Astrophys. J.* (in press, preprint astro-ph/0003289).
- [65] Bower, R.G., Benson, A.J., Baugh, C.M., Cole, S., Frenk, C.S. & Lacey, C.G. The Impact of Galaxy Formation on the  $X$ -Ray Evolution of Clusters. *Mon. Not. R. Astr. Soc.* (submitted, preprint astro-ph/0006109).
- [66] Bartlett, J.G. Sunyaev-Zel'dovich Surveys: Analytic treatment of cluster detection. *Astron. Astrophys.* (in press, preprint astro-ph/0001267).
- [67] Carlstrom, J.E. *Physica Scripta Volume T* **85**, 148–155 (2000).
- [68] Górski, K.M., Banday, A.J., Bennett, C.L., Hinshaw, G., Kogut, A., Smoot, G.F., Wright, E.L. Power Spectrum of Primordial Inhomogeneity Determined from the Four-Year COBE DMR Sky Maps. *Astrophys. J. Lett.* **464**, L11–L14 (1996).

- [69] Bahcall, N. A., Ostriker, J. P., Perlmutter, S., Steinhardt, P. J. The Cosmic Triangle: Revealing the State of the Universe. *Science* **284**, 1481–1488 (1999).
- [70] Rosati, P., Borgani, S., Della Ceca, R., Stanford, A., Eisenhardt P., & Lidman, C. The Most Distant  $X$ -ray Clusters and the Evolution of their Space Density. in *Large Scale Structure in the X-ray Universe*, held in Santorini, Greece, p.13–20 (2000).
- [71] Gioia, I. Cluster Surveys. in *constructing the Universe with Galaxy Clusters*, held in Paris, France (in press, preprint astro-ph/0010059).
- [72] Rosati, P. Stanford, S.A., Eisenhardt, P.R., Elston, R., Spinrad, H., Stern, D. & Dey, A. An  $X$ -Ray Selected Galaxy Cluster at  $z = 1.26$ . *Astron. J.* **118**, 76–85 (1999).
- [73] Suto, Y., Yamamoto, K., Kitayama, T. & Jing, Y.P. Two-Point Correlation Functions of X-Ray-Selected Clusters of Galaxies: Theoretical Predictions for Flux-Limited Surveys. *Astrophys. J.* **534**, 551 (2000).
- [74] Moscardini, L., Matarrese, S., Lucchin, F., & Rosati, P. Predicting the Clustering of  $X$ -Ray Selected Galaxy Clusters in Flux-Limited Surveys. *Mon. Not. R. Astron. Soc.* (in press).
- [75] <http://xmm.vilspa.esa.es>
- [76] Burrows C.J., Burg R., & Giacconi R. Optimal grazing incidence optics and its application to wide-field  $X$ -ray imaging. *Astrophys. J.* **392**, 760–765 (1992).
- [77] Eisenstein, D.J. & Hu, P. Baryonic Features in the Matter Transfer Function. *Astrophys. J.* **496**, 605–614 (1998).

- [78] Eke, V.R., Cole, S., Frenk, C.S. Cluster evolution as a diagnostic for  $\Omega$ . *Mon. Not. R. Astron. Soc.* **282**, 263–280 (1996).
- [79] Girardi, M., Borgani, S., Giuricin, G., Mardirossian, F., Mezzetti, M. The Observational Mass Function of Nearby Galaxy Clusters. *Astrophys. J.* **506**, 45–52 (1998).
- [80] Viana, P.T.P., Liddle, A.R. Galaxy clusters at  $0.3 < z < 0.4$  and the value of  $\Omega_0$ . *Mon. Not. R. Astron. Soc.* **303**, 535–545 (1999).
- [81] Borgani, S., Rosati, P., Tozzi, P., Norman, G. Cosmological Constraints from the ROSAT Deep Cluster Survey. *Astrophys. J.* **517**, 40–53 (1999).
- [82] Margon, B. The Sloan Digital Sky Survey. *Phil. Trans. R. Soc. Lond. A* (preprint astro-ph/9805314).
- [83] Folkes, S.R., Ronen, S., Price, I., Lahav, O., Colless, M. et al. (the 2dF team) The 2dF Galaxy Redshift Survey: spectral types and luminosity functions. *Mon. Not. R. Astron. Soc.* **308**, 459–472 (1999).
- [84] Burles, S. & Tytler, D. The Deuterium Abundance toward Q1937-1009. *Astrophys. J.* **499**, 699–712 (1998).
- [85] Hoyle, F., Baugh, C.M., Shanks, T. & Ratcliffe, A. The Durham/UKST Galaxy Redshift Survey - VI. Power spectrum analysis of clustering. *Mon. Not. R. Astr. Soc.* **309**, 659–671 (1999).
- [86] Mellier, Y. Probing the Universe with Weak Lensing. *ARA&A* **37**, 127–(1999).

## Acknowledgments

We thank the REFLEX collaboration for giving us the possibility to discuss material in advance of publication; Chris Collins, Fabio Governato and Meg Urry

for reading the manuscript; Davide Lazzati and Alberto Moretti for their help with some of the figures; and Marisa Girardi for providing the data files on which Fig. 5 is based. We also acknowledge several enlightening discussions on  $X$ -ray clusters with Piero Rosati.

## Box 1: A large-scale structure primer

The *redshift*  $z$  of a galaxy is defined as the fractional increase in the observed wavelength of the emitted radiation with respect to its laboratory value:  $z = (\lambda - \lambda_o)/\lambda_o$ . In the standard cosmological model this is interpreted as due to the global expansion of the Universe, and to first approximation (i.e., neglecting any acceleration of the cosmic expansion) it can be thought as the consequence of a recession velocity  $v_{rec} = cz$  (where  $c$  is the speed of light), proportional to the distance to the galaxy itself,  $v_{rec} \simeq H_o d$ . This is the empirically verified *Hubble law* and the constant of proportionality  $H_o$  is the famous *Hubble constant*. Through this relation, we can measure the distance to far-away galaxies by simply observing the red-shift in their spectrum.

According to the picture of gravitational instability, cosmic structures arise from the gravitational growth on initially tiny inhomogeneities, generated in the very early stages of the Universe life. These cosmic inhomogeneities are described by the fluctuation field  $\delta(\vec{x}, z) = (\delta\rho/\rho)_{\vec{x}, z}$ , where  $\rho(\vec{x}, z)$  is the density of the Universe at the point  $\vec{x}$  and at redshift  $z$ . A basic statistical characterization of  $\delta(\vec{x})$  is represented by its two-point correlation function,  $\xi(r)$ , which describes the excess fluctuations with respect to a uniform distribution. The Fourier transform of  $\xi(r)$  is the power spectrum

$$P(k) = \frac{1}{2\pi^2} \int_0^\infty dr \xi(r) \frac{\sin kr}{kr}. \quad (1)$$

The power spectra of two representative cosmological models are compared in Fig. 2 to observational results. Even keeping fixed the assumption of a Universe dominated by Cold Dark Matter (CDM), different shapes for the matter  $P(k)$

can be obtained by varying the values of  $\Omega_m$ ,  $h$  and the amount of baryons [77]. Its amplitude is instead usually determined in a phenomenological way, by matching some observed measure of the root-mean-squared (*rms*) fluctuation (in the mass, not in the light!) at some scale. One way is to reproduce the level of CMB anisotropy measured by the *COBE* satellite [68], that probes fluctuations on scales  $\sim 10^3 \text{Mpc}$ . On a completely different range of scales, an alternative method is offered by the local abundance of galaxy clusters, in virtue of their ability to probe the mass fluctuations. Since they formed from the collapse of density fluctuations on a scale  $\simeq 10 h^{-1} \text{Mpc}$ , their number density today is directly proportional to the *rms* amplitude of such fluctuations at the onset of their growth. As massive clusters arise from rare high peaks of the density fluctuation field, their number density is rather sensitive to the amplitude of these fluctuations, providing a precise constraint on the amplitude of  $P(k)$  [78, 79, 80, 69]. For instance, the simulations shown in Fig. 6 refer to two models having different  $\Omega_m$  but normalisation tuned so as to produce a comparable number of clusters at  $z = 0$ .

Once  $P(k)$  is normalised at the present time, its amplitude in the past depends on the evolution of density fluctuations. As long as fluctuations are small, their growth is independent of the position, so that  $\delta(\vec{x}, z) = D(z)\delta(\vec{x}, z = 0)$ . The redshift dependence of  $D(z)$  is determined by comparing the time-scales for gravitational collapse of a perturbation and for the expansion of the Universe [25, 26]. These two time scales are actually always identical when  $\Omega_m = 1$ , thus implying that the perturbation growth equals the cosmic expansion factor:  $D(z) = (1 + z)^{-1}$ . For a low-density Universe, the two time-scales are similar at early epochs, while the cosmic expansion overtakes the fluctuation growth when the former stops feeling the self-gravity of the Universe. This happens at an epoch corresponding to  $1 + z \simeq \Omega_m^{-1/3}$  or  $1 + z \simeq \Omega_m^{-1}$  in the cases with and without a cosmological constant providing flat geometry, respectively. Therefore, in a low- $\Omega_m$  Universe the fluctuations growth progressively slows down at later epochs and eventually freezes.

The plots in Fig. 6 clearly show the different degree of evolution characterising models with different values of  $\Omega_m$ , as witnessed by the different number of clusters already formed at high redshift. For this reason, the determination of the number density of distant clusters is a powerful diagnostic for cosmological models (see refs.[81, 62] and references therein).

## Figures

### Figure 1:

Maps of the cosmic web. The top panel shows the distribution of  $\sim 26,000$  galaxies in the Northern and Southern slices of the Las Campanas Redshift Survey[19] (LCRS), to a maximum distance of  $600 h^{-1}\text{Mpc}$  from the observer, located in the centre. The typical morphology of large-scale structure, with filaments and voids is evident. Superimposed on the “blue dust” of the galaxy distribution, the green circles mark the positions of those  $X$ -ray clusters of galaxies from the REFLEX survey [13] that lie approximately within the volume of the LCRS. The full volume of the REFLEX survey (which contains all clusters brighter than an  $X$ -ray flux of  $3 \times 10^{-12} \text{ erg s}^{-1} \text{ cm}^{-2}$  over a large part of the southern sky) within the same distance limit, is shown in the bottom panel (similar orientation, South is up for clarity). The much larger volume sampled by clusters and their clustering along filamentary structures is evident. The missing part of the hemisphere corresponds to the region highly obscured by the Milky Way disk ( $\pm 20^\circ$  in galactic latitude). Similar volumes will be partly filled by galaxy redshift measurements only in the coming years [82, 83].

### Figure 2:

Statistical description of clustering. The two-point correlation functions  $\xi$  of galaxies (squares) and  $X$ -ray clusters of galaxies (circles), computed from the two data sets of Fig. 1 [21, 32], plotted as a function of separation  $r_s$  (where



the suffix  $s$  indicates that all object distances are computed from the measured redshift). The curves are the predictions of two CDM models, with different density parameters  $\Omega_m$ , for an  $X$ -ray cluster survey with the same flux-limit as the real data. Solid curve:  $\Omega_m = 0.3$  and Hubble parameter  $h = 0.7$ ; dashed curve:  $\Omega_m = 0.5$  and  $h = 0.6$ . Both models have flat spatial geometry provided by a cosmological constant contribution (i.e.  $\Omega_m + \Omega_\Lambda = 1$ ) and power-spectrum normalization chosen so as to be consistent measured CMB anisotropies [68, 15, 16]. Also, we take  $\Omega_{bar}h^2 = 0.019$  for the baryon density [84].

### Figure 3:

The power spectrum of the distribution of galaxies and  $X$ -ray clusters of galaxies from the data of Fig. 1. The squares are from galaxy data, which in addition to the LCRS points (filled squares [27]), include a measure from another survey with better volume coverage (open squares [85]). The filled circles show instead an estimate of the power spectrum of  $X$ -ray selected clusters from the REFLEX survey [33]. Note the rather different amplitude between the galaxy and cluster power spectra, similarly to that shown by correlation functions (see Fig. 2). The two curves are theoretical predictions from the same cosmological models shown in Fig. 2.

### Figure 4:

The visual and  $X$ -ray appearance of the rich galaxy cluster RXCJ1206.2-0848 at redshift  $z = 0.44$ , discovered by the REFLEX survey [31]. The optical image has been obtained by combining three images taken with the ESO 3.6 m telescope, corresponding to the red, green and blue bands. The yellowish colour of objects in the central region reflects the old stellar population characterising elliptical galaxies, that typically dominate in cluster cores. Note also the presence of at least two probable gravitational arcs (with blue colour), near the central giant elliptical galaxy. These are the result of the *gravitational lensing* phenomenon, by

which the cluster mass distorts and amplifies the images of background galaxies (thus providing an independent way to probe its potential [86]). The contours show the  $X$ -ray emission from the cluster measured by the ROSAT All-Sky Survey, which yield a luminosity  $L_X \simeq 5 \times 10^{44} h^{-2} \text{ erg s}^{-1}$ . The field of view in this image is about 5 arcmin, corresponding to a physical size of  $\sim 1 h^{-1} \text{ Mpc}$  at the cluster distance.

### Figure 5:

Correlations between mass and observational properties of galaxy clusters. The correlations with Abell [1, 2] richness counts  $N_c$  (upper panel) and their  $X$ -ray bolometric luminosity  $L_{X,bol}$  (lower panel), based on the merge of a compilation of clusters with accurate measures of velocity dispersion [40] and a sample of  $X$ -ray bright Abell clusters (XBACs [10]). Cluster masses are estimated by applying the virial theorem to the velocity dispersions of member galaxies. In both panels, filled circles are for those clusters belonging to XBACs, while open circles are for those Abell clusters that have too low a  $X$ -ray emission to be included in XBACs. The weak correlation in the upper panel demonstrates the difficulty of using clusters selected by optical richness to strongly constrain cosmological scenarios. This aim is better achieved with clusters selected by  $X$ -ray luminosity, which clearly shows a tighter correlation with the cluster mass.

### Figure 6:

The evolution of gravitational clustering simulated using an N-body code for two different models. Each of the three redshift snapshots shows a region with  $250 h^{-1} \text{ Mpc}$  side and  $75 h^{-1} \text{ Mpc}$  thick (co-moving with the cosmic expansion). Each simulation contains about two millions particles. The upper one describes a flat low-density model with  $\Omega_m = 0.3$  and  $\Omega_\Lambda = 0.7$  (L03), while the lower an Einstein-de-Sitter model (EdS) with  $\Omega_m = 1$ . In both cases the amplitude of the power spectrum is consistent with the number density of nearby galaxy clusters

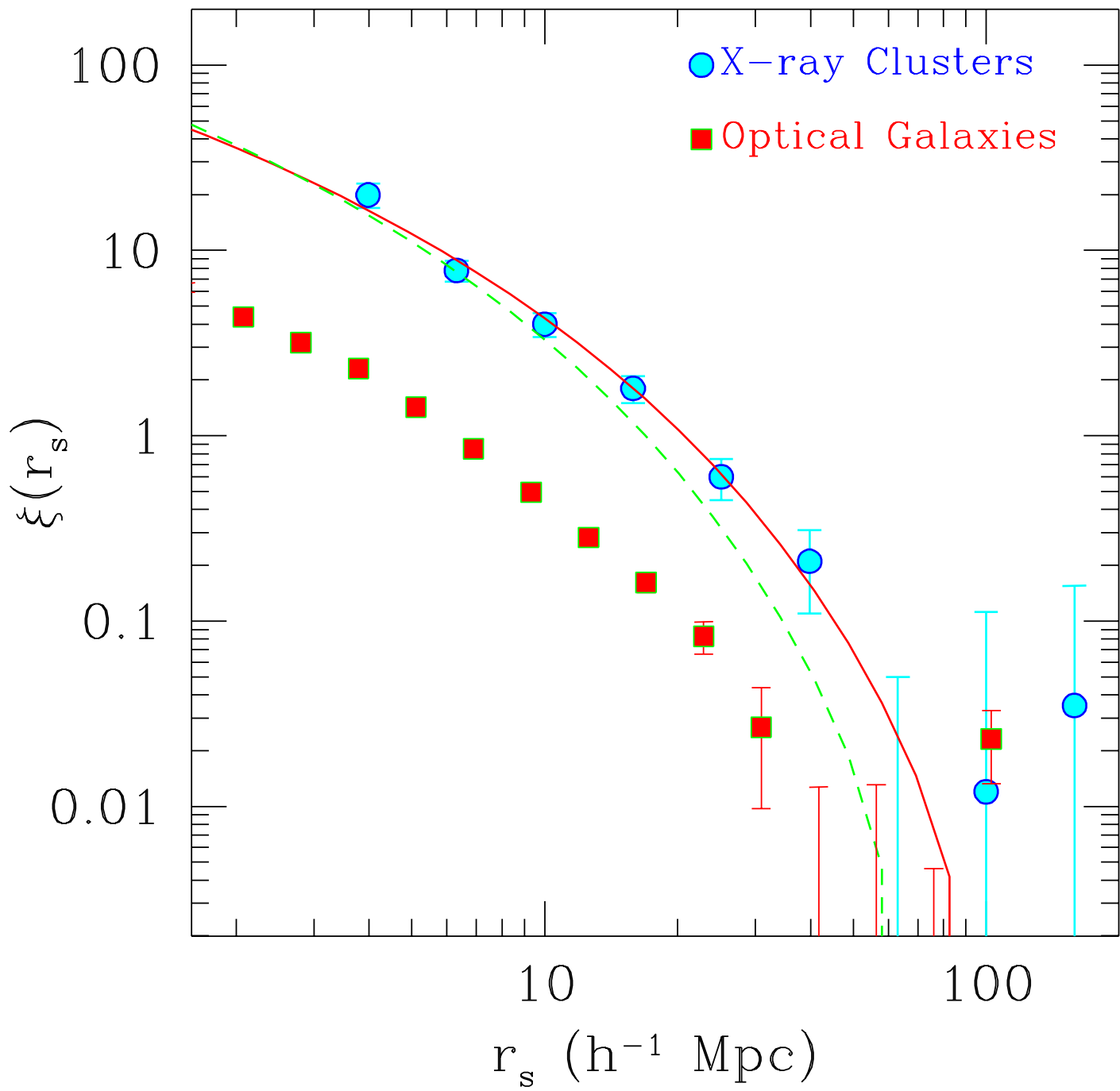
[78, 79] and with the large-scale CMB anisotropies [68]. Superimposed on the dark matter distribution, the yellow circles mark the positions of galaxy clusters that would be seen shining in  $X$ -rays with a temperature  $T > 3$  keV, as computed from the cluster mass according to the relation calibrated from hydrodynamical simulations [56]. The size of the circles is proportional to temperature.

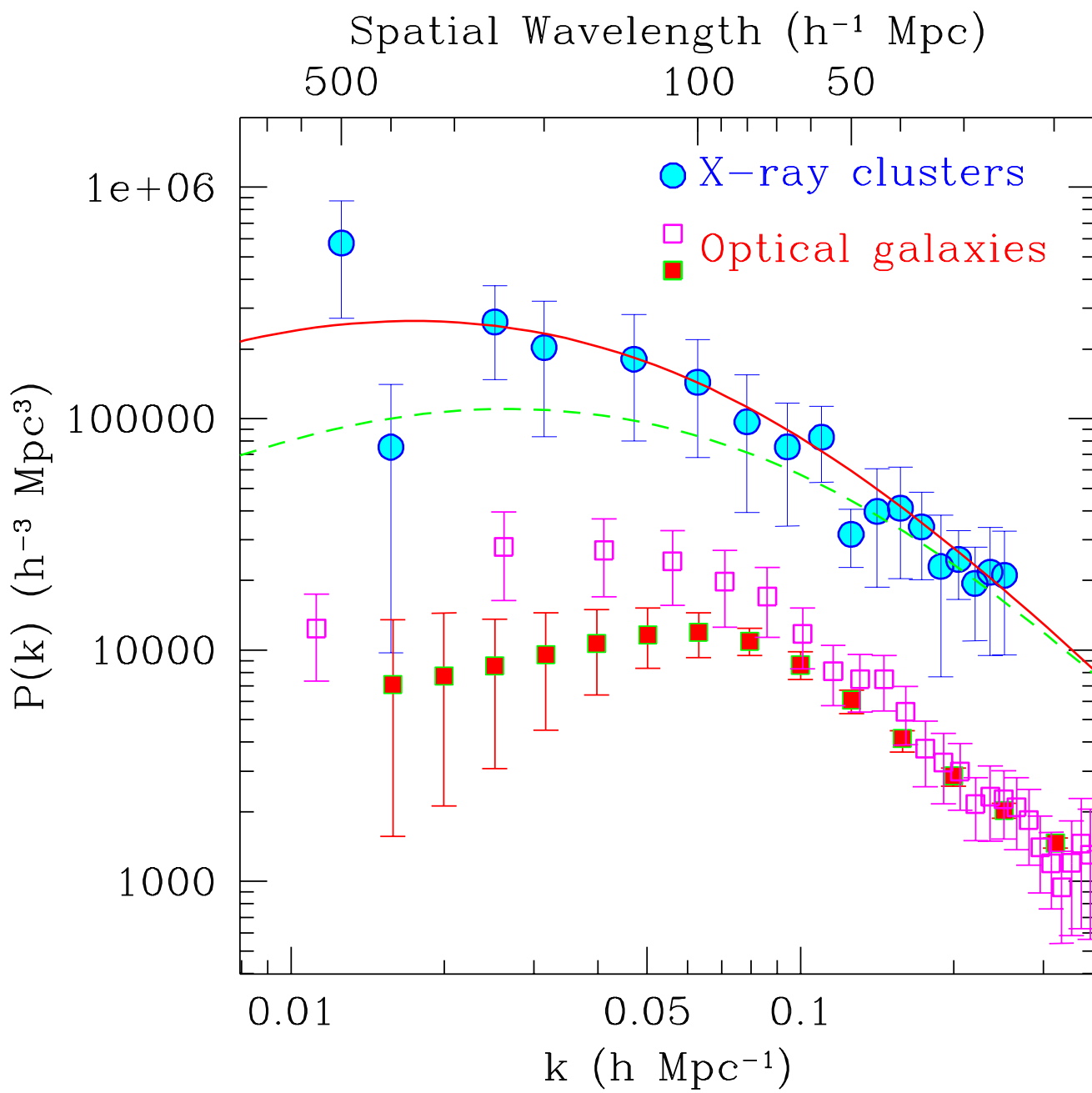
This figure "fig1\_bottom.gif" is available in "gif" format from:

<http://arxiv.org/ps/astro-ph/0012439v1>

This figure "fig1\_top.gif" is available in "gif" format from:

<http://arxiv.org/ps/astro-ph/0012439v1>

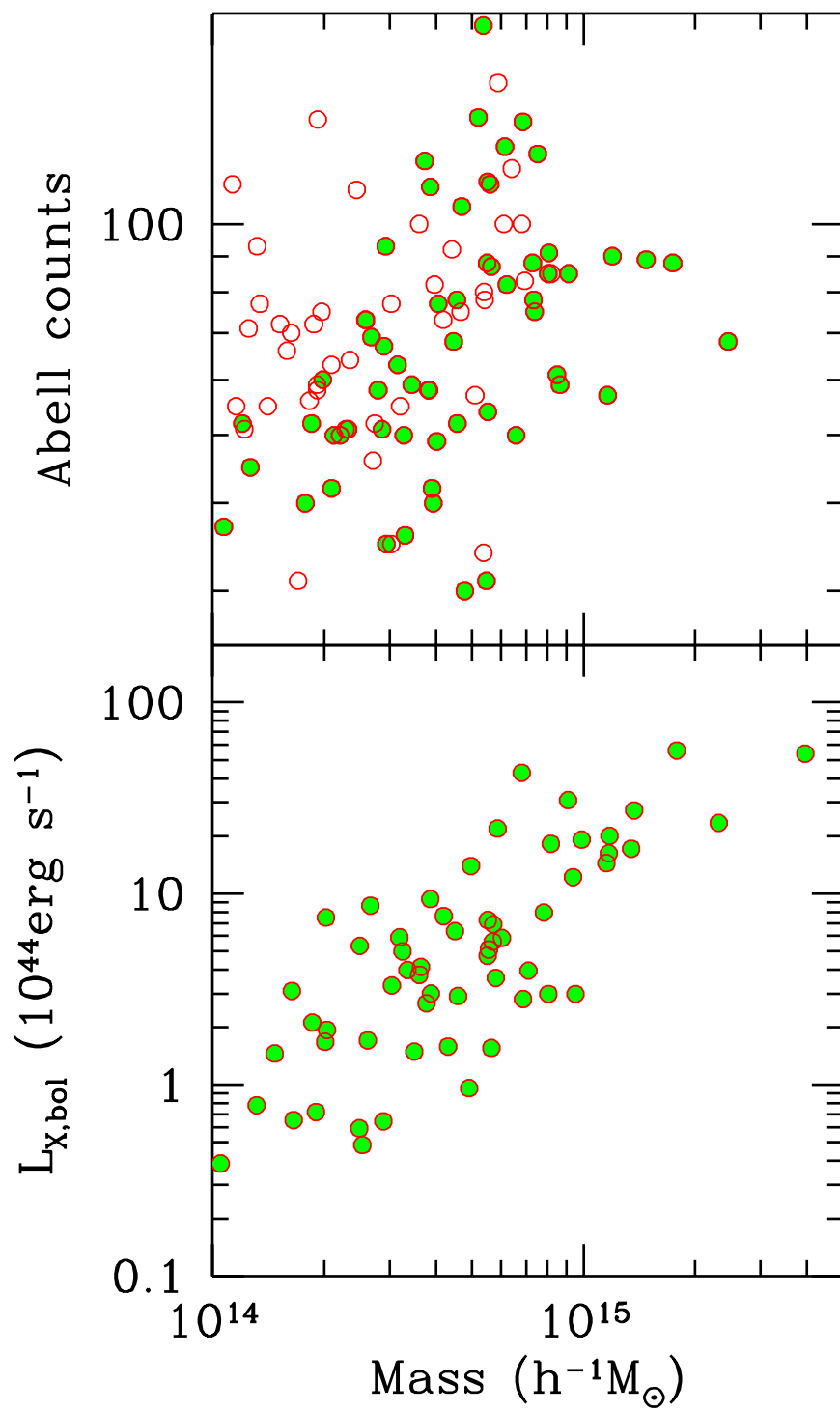




This figure "fig4.gif" is available in "gif" format from:

<http://arxiv.org/ps/astro-ph/0012439v1>





This figure "fig6.gif" is available in "gif" format from:

<http://arxiv.org/ps/astro-ph/0012439v1>